Electronic Supplementary Material (ESI) for Journal of Materials Chemistry C.

Supporting Information

Phase transition regulation and piezoelectric performance optimization of fresnoite crystal for high temperature acceleration sensing

Chao Jiang[a], Caizi Zhang[b], Fangfei Li[b], Li Sun[a], Yanlu Li[a], Fapeng Yu[a] *, and Xian Zhao[a]

[a] Key Laboratory of Laser & Infrared System, Ministry of Education, State Key Laboratory of Crystal Materials, Shandong University, Jinan, China

[b] State Key Laboratory of Superhard Materials, College of Physics, Jilin University, Changchun, China

Email addresses: fapengyu@sdu.edu.cn

Table S1. Atomic Coordinates and equivalent isotropic displacement parameters for $Ba_{2-x}Sr_xTS$ crystals

$Ba_2TiSi_2O_8$				
Atom	*x*	*y*	*z*	U_{eq} (Å^2×10^3)
Ba1	0.8271(0)	0.3271(0)	0.0007(1)	12.33(17)
Ti1	0.5000	0.5000	0.5358(3)	9.6(3)
Si1	0.6280(1)	0.1280(1)	0.5141(6)	9.7(3)
O1	0.5759(7)	0.2927(6)	0.6445(10)	24.9(10)
O2	0.6261(4)	0.1261(4)	0.2068(12)	12.2(9)
O3	0.5000	0.0000	0.6390(19)	24.8(19)
O4	0.5000	0.5000	0.2132(19)	19.6(16)

Symmetry operations: (#1) x,y,z; (#2) -y,x,z; (#3) -x,-y,z; (#4) y,-x,z; (#5) 1/2-x,1/2+y,z; (#6) 1/2+x,1/2-y,z; (#7) 1/2-y,1/2-x,z; (#8) 1/2+y,1/2+x,z

$Ba_{1.8}Sr_{0.2}TiSi_2O_8$				
Atom	*x*	*y*	*z*	U_{eq} (Å^2×10^3)
Ba1	0.82712(2)	0.32712(2)	0.19339(8)	14.23(9)
Sr1	0.82712(2)	0.32712(2)	0.19339(8)	14.23(9)
Ti1	0.5000	0.5000	0.7274(2)	11.7(3)
Si1	0.62803(3)	0.12803(3)	0.7048(4)	11.7(2)
O1	0.5764(5)	0.2923(4)	0.8370(7)	29.8(8)
O2	0.6264(3)	0.1264(6)	0.3988(7)	14.9(6)
O3	0.5000	0.0000	0.8231(11)	29.0(14)
O4	0.5000	0.5000	0.4024(19)	22.4(11)

Symmetry operations: (#1) x,y,z; (#2) -x,-y,z; (#3) -y,x,z; (#4) y,-x,z; (#5) x+1/2,-y+1/2,z; (#6) -x+1/2,y+1/2,z; (#7) -y+1/2,-x+1/2,z; (#8) y+1/2,x+1/2,z

$Ba_{1.6}Sr_{0.4}TiSi_2O_8$				
Atom	*x*	*y*	*z*	U_{eq} (Å^2×10^3)
Ba1	0.17286(2)	0.67286(2)	0.99873(7)	13.96(10)

Sr1	0.17286(2)	0.67286(2)	0.99873(7)	13.96(10)
Ti1	0.5000	0.5000	0.4657(2)	12.6(2)
Si1	0.37192(11)	0.87192(11)	0.4886(4)	13.0(2)
O1	0.4240(6)	0.7074(4)	0.3555(7)	34.2(10)
O2	0.3739(4)	0.8739(6)	0.7958(8)	16.4(7)
O3	0.5000	1.0000	0.3689(12)	34.6(19)
O4	0.5000	0.5000	0.7918(12)	23.7(13)

Symmetry operations: (#1) x,y,z; (#2) -x,-y,z; (#3) x+1/2,-y+1/2,z; (#4) -x+1/2,y+1/2,z; (#5) -y,x,z; (#6) y,-x,z; (#7) y+1/2,x+1/2,z; (#8) -y+1/2,-x+1/2,z

$Ba_{1.4}Sr_{0.6}TiSi_2O_8$				
Atom	*x*	*y*	*z*	U_{eq} (Å^2×10^3)
Ba1	0.32706(7)	0.82706(7)	0.00096(15)	19.0(6)
Sr1	0.32706(7)	0.82706(7)	0.00096(15)	19.0(6)
Ti1	0.50000	0.50000	0.5331(9)	16.5(10)
Si1	0.1281(3)	0.6281(3)	0.5100(7)	17.7(9)
O1	0.0000	0.5000	0.629(3)	44.0(6)
O2	0.1264 (7)	0.6264(9)	0.203(3)	19.0(2)
O3	0.2920(15)	0.5759(17)	0.644(2)	43.0(16)
O4	0.50000	0.50000	0.206(5)	38.0(5)

Symmetry operations: (#1) x,y,z; (#2) -y,x,z; (#3) -x,-y,z; (#4) y,-x,z; (#5) -x+1/2,y+1/2,z; (#6) x+1/2,-y+1/2,z; (#7) -y+1/2,-x+1/2,z; (#8) y+1/2,x+1/2,z

Table S2. Chemical composition of grown $Ba_{2-x}Sr_xTS$ crystal

		Measured value	Theoretical value
X=0.2	BaO	57.670%	55.558%
	SrO	3.923%	4.172%
X=0.4	BaO	50.891%	49.385%
	SrO	8.219%	8.344%
X=0.6	BaO	43.485%	43.212%

	SrO	12.434%	12.515%

Table S3. Thermal expansion coefficient for $Ba_{2-x}Sr_xTS$ crystals

Unit ($10^{-6}K^{-1}$)	Before phase transition		After phase transition	
	X	Z	X	Z
x=0	7.96	2.30	7.98	15.0
x=0.2	8.54	3.66	8.58	13.14
x=0.4	7.78	4.59	8.99	13.07
x=0.6	8.39	4.74	8.00	12.48

Table S4. Bond distances and bond valence sum for $Ba_{2-x}Sr_xTS$ crystals

$Ba_2TiSi_2O_8$					
Ba-O1	2.993	Ti1-O1	1.963	Si1-O1	1.620
Ba-O1	2.993	Ti1-O1	1.963	Si1-O1	1.620
Ba-O1	2.845	Ti1-O1	1.963	Si1-O2	1.599
Ba-O1	2.845	Ti1-O1	1.963	Si1-O3	1.657
Ba-O2	2.791	Ti1-O4	1.678		
Ba-O2	2.791				
Ba-O2	2.647				
Ba-O3	2.835				
1.8469		4.1294		4.0063	

$Ba_{1.8}Sr_{0.2}TiSi_2O_8$

Ba-O1	2.838	Sr-O1	2.838	Ti1-O1	1.964	Si1-O1	1.617
Ba-O1	2.838	Sr -O1	2.838	Ti1-O1	1.964	Si1-O1	1.617
Ba-O1	2.990	Sr -O1	2.990	Ti1-O1	1.964	Si1-O2	1.588
Ba-O1	2.990	Sr -O1	2.990	Ti1-O1	1.964	Si1-O3	1.657
Ba-O2	2.637	Sr -O2	2.637	Ti1-O4	1.687		
Ba-O2	2.786	Sr -O2	2.786				
Ba-O2	2.786	Sr -O2	2.786				
Ba-O3	2.830	Sr -O3	2.830				
1.8780		1.1959		4.0874		4.0551	

$Ba_{1.6}Sr_{0.4}TiSi_2O_8$							
Ba-O1	2.837	Sr-O1	2.837	Ti1-O1	1.961	Si1-O1	1.619
Ba-O1	2.837	Sr -O1	2.837	Ti1-O1	1.961	Si1-O1	1.619
Ba-O1	2.985	Sr -O1	2.985	Ti1-O1	1.961	Si1-O2	1.591
Ba-O1	2.985	Sr -O1	2.985	Ti1-O1	1.961	Si1-O3	1.658
Ba-O2	2.776	Sr -O2	2.776	Ti1-O4	1.689		
Ba-O2	2.776	Sr -O2	2.776				
Ba-O2	2.632	Sr -O2	2.632				
Ba-O3	2.825	Sr -O3	2.825				
1.9058		1.2138		4.1015		4.0327	

$Ba_{1.4}Sr_{0.6}TiSi_2O_8$							
Ba-O1	2.833	Sr-O1	2.833	Ti1-O1	1.972	Si1-O1	1.622
Ba-O1	2.833	Sr -O1	2.833	Ti1-O1	1.972	Si1-O1	1.622
Ba-O1	2.979	Sr -O1	2.979	Ti1-O1	1.972	Si1-O2	1.598
Ba-O1	2.979	Sr -O1	2.979	Ti1-O1	1.972	Si1-O3	1.662
Ba-O2	2.773	Sr -O2	2.773	Ti1-O4	1.70		
Ba-O2	2.773	Sr -O2	2.773				
Ba-O2	2.623	Sr -O2	2.623				

Ba-O3	2.828	Sr -O3	2.828				
1.9277		1.2275		3.98138		3.9860	

The phase transition for BTS crystal was characterized taking advantage of the in-situ high temperature TEM tests. In-situ high temperature transmission electron microscope (TEM) was conducted using a Titan Cubed Themis G2-300 (FEI) with a condenser spherical aberration corrector operating at an accelerating voltage of 200 kV. The BTS crystal sample was prepared by Focused Ion beam (FIB) using Helios NanoLab 460HP (FEI) and the diffraction patterns were recorded along $[2\bar{1}0]$-oriention.

Results are shown in Figure S1, where obvious satellite reflections are observed at room temperature. The appearance of satellite reflections in the electron diffraction pattern proves that the BTS crystal is an incommensurate phase at room temperature. When the temperature rising up to 150^{o}C, the intensity of the satellite reflections gradually weakens and disappears completely prior to 200^{o}C, only the main reflection points can be observed, indicating the BTS crystal is a normal phase at high temperature above 150^{o}C. Based on the in-situ high temperature TEM results, it can be confirmed that the phase transition type of the BTS crystal in the vicinity of 150^{o}C is “incommensurate phase-normal phase transition”.

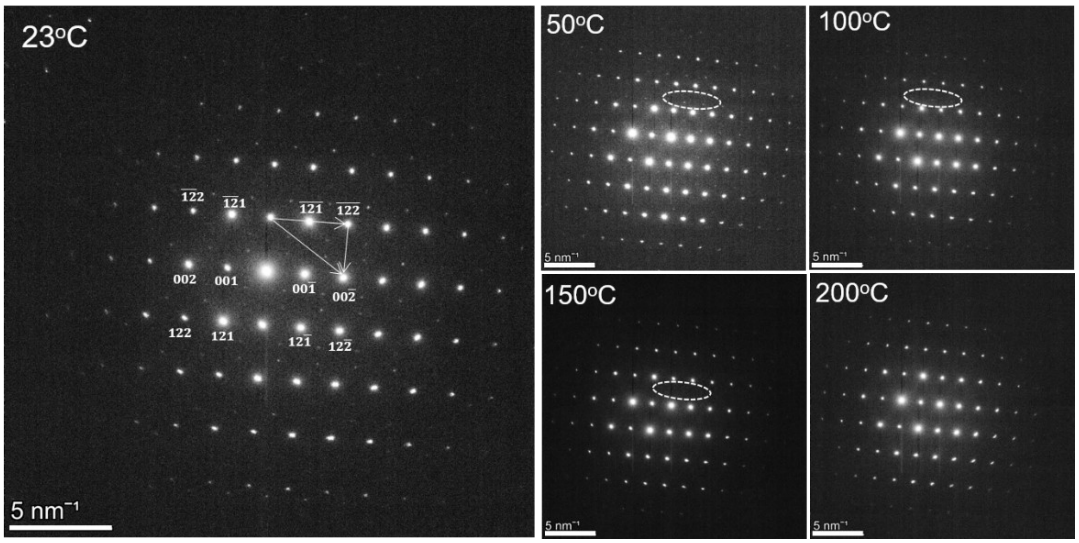

Figure S1. In- situ high temperature electron diffraction patterns collected from BTS single crystal sample

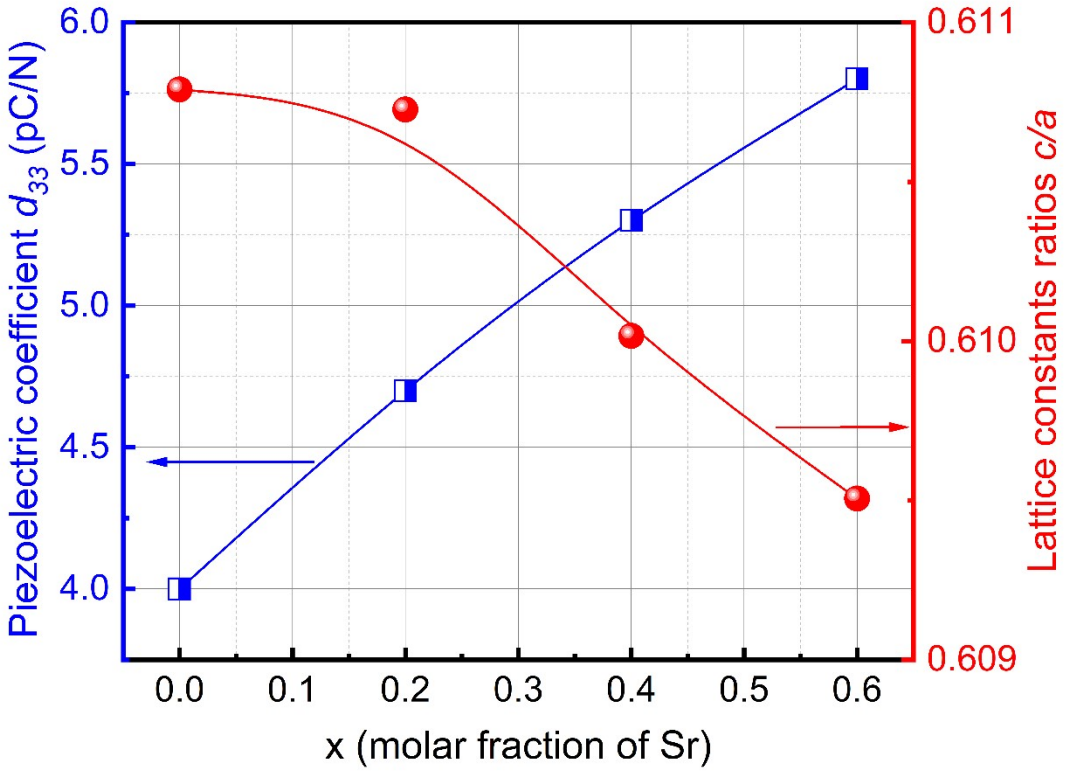

Figure S2. Piezoelectric coefficient d_{33} and lattice constants ratio c/a versus molar fraction of Sr

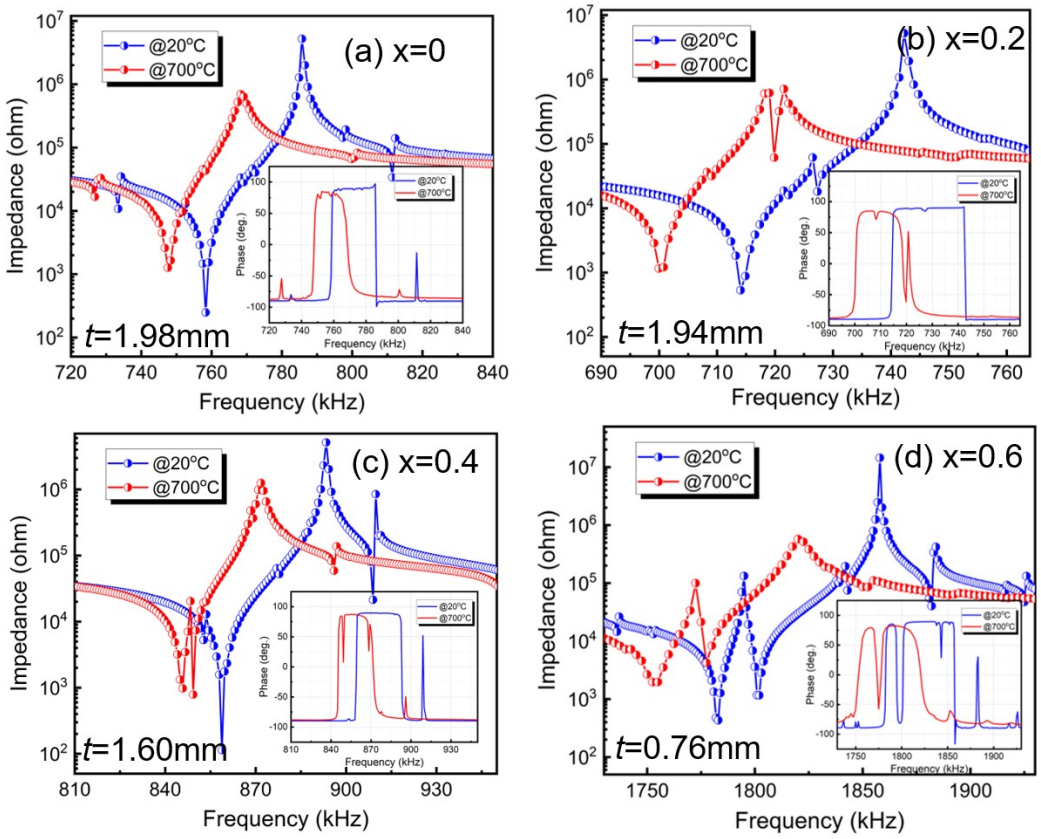

Figure S3. Impedance spectra and phase angles of thickness shear mode d_{15}.

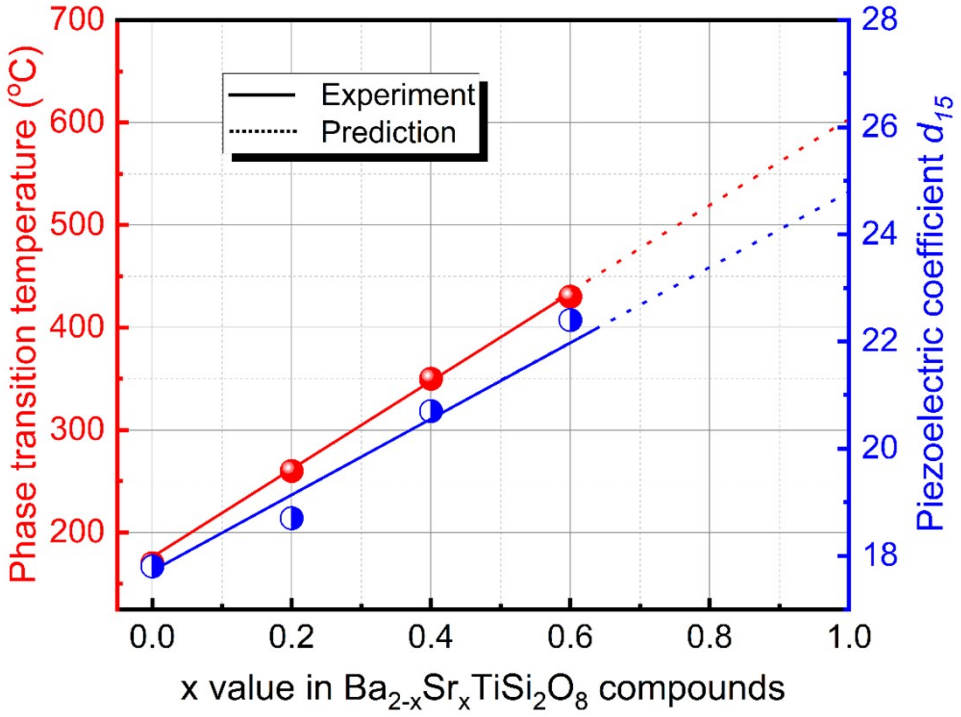

Figure S4. Phase transition temperature and piezoelectric coefficient d_{15} as a function of molar fraction of Sr.

The polycrystalline were checked by X-ray diffraction (XRD) pattern using the Rigaku X-ray diffractometer (Rigaku, The Woodlands, TX) with CuKα radiation (λ=1.5418Å) and nickel filter in a wide range of 2θ from 15° to 80° with a scanning rate of 2° min^{-1}. The instrument was calibrated using the pure silicon sample provided with the instrument. The lattice parameters and other detailed structural information were obtained by the Rietveld refinement Fullprof program using a pseudo-Voigt function. The Rietveld refined profiles are shown in figure S4, where the observed pattern is consistent with the calculated pattern using the Rietveld analysis. It is noticed that a minor peak was observed at 2θ=32.34° for x=0.9 component, which matches the highest intensity peak of $SrTiO_3$, (JCPDF No: #35-0734).

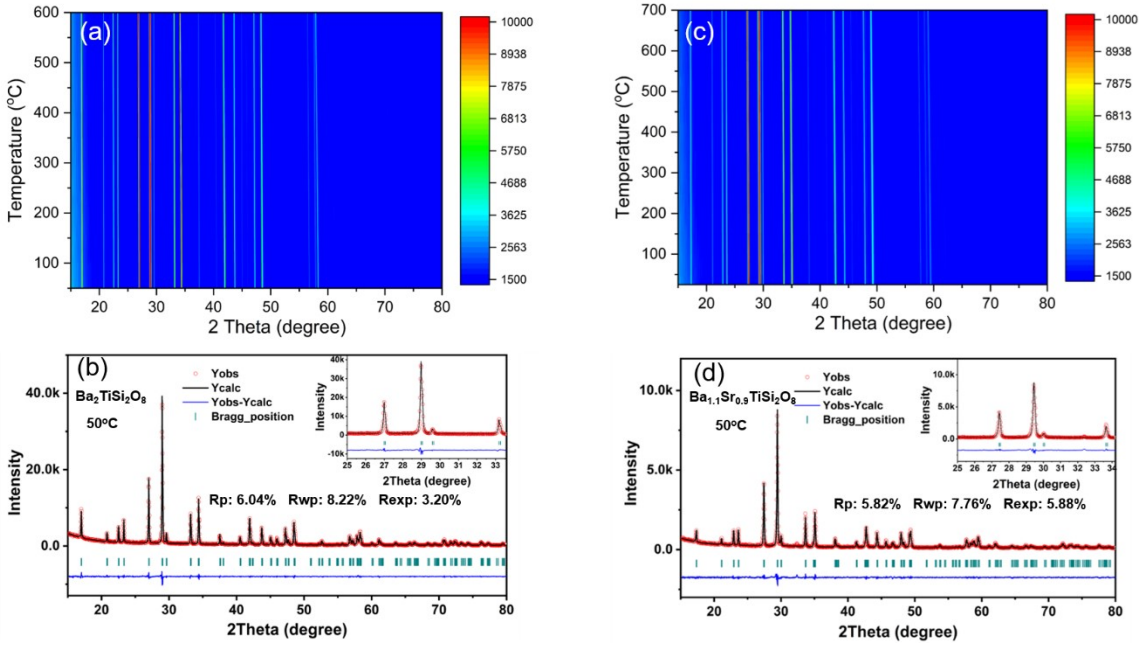

Figure S5. In-situ high temperature X-ray diffraction patterns of $Ba_2TiSi_2O_8$ (a) and Rietveld refined profile example of $Ba_2TiSi_2O_8$ at 50°C (b); In-situ high temperature X-ray diffraction patterns of $Ba_{1.1}Sr_{0.9}TiSi_2O_8$ (c) and Rietveld refined profile example of $Ba_{1.1}Sr_{0.9}TiSi_2O_8$ at 50°C (d)